

Research Paper

Exploring the Limits of Machine-Learning Classification of Neutron-Star Matter Models

Wasif Husain

School of Science, Technology and Engineering, University of Sunshine Coast, 182, Victoria Square Adelaide 5000

Abstract

We investigate the extent to which supervised machine-learning techniques can distinguish between neutron-star matter models using macroscopic and oscillation-related quantities derived from theoretical stellar configurations. Four representative matter scenarios nucleonic, hyperonic, dark-matter-admixed, and strange-matter models are considered, and a synthetic dataset is constructed from solutions of the Tolman–Oppenheimer–Volkoff equations under fixed microphysical and transport assumptions.

A shallow neural-network classifier is trained on physically motivated features, including gravitational mass, stellar radius, and oscillation-related quantities, to evaluate classification performance across the model space. Rather than aiming at unique composition inference, the analysis focuses on identifying regimes of distinguishability and intrinsic degeneracy between models. We find that certain matter scenarios can be separated under controlled assumptions, while others exhibit substantial overlap, reflecting fundamental similarities in their effective equations of state.

These results demonstrate that machine learning provides a useful computational framework for mapping the limits of model classification in neutron-star studies, clarifying where inference is feasible and where it remains intrinsically model dependent. The methodology is readily extensible to more complex microphysics and to future multi-messenger datasets.

Keywords: Neutron Stars, Equation of State, Machine Learning, Neural Networks, Dark Matter, Hyperons, Strange Matter.

1. Introduction

Neutron stars provide a unique laboratory for dense strongly interacting matter Lattimer and Prakash (2004); Özel and Freire (2016), probing energy densities well beyond nuclear saturation. A wide range of microphysical scenarios have been proposed for their interiors, including purely nucleonic matter, hyperon-rich matter, deconfined strange quarks, and neutron decays into non-interactive dark-matter configurations. Among dark-matter scenarios, we focus on a neutron-decay model in which neutrons convert into a non-self-interacting dark component that couples to baryonic matter only gravitationally.

Each scenario imprints characteristic signatures on macroscopic observables such as the mass-radius (M - R) relation and the f -mode frequency (Andersson and Kokkotas (1998); Doneva et al. (2015); Kokkotas and Schmidt (1999)), which can be constrained by X-ray timing, radio pulsar measurements, and gravitational waves from binary mergers.

Traditional studies proceed by specifying an equation of state (EOS), solving the Tolman–Oppenheimer–Volkoff (TOV) equations for hydrostatic equilibrium, and comparing the resulting M - R curves with observational constraints. In recent years, machine learning (ML) techniques have been deployed in neutron star physics (Fujimoto et al. (2018); Morawski and Bejger (2020); Raithel et al. (2017); Krastev (2022); Soma et al. (2023)), targeting tasks such as EOS reconstruction from mock observations Fujimoto et al. (2021), probabilistic inference of the speed-of-sound profile, or mapping between observational posteriors and

internal structure parameters. These approaches demonstrate that ML can encapsulate complex non-linear relationships between the EOS and observables, but often rely on high-dimensional EOS parametrisations or large training sets.

In this work, a deliberately simple and transparent objective is pursued: given synthetic stellar observables generated from four distinct EOS families: nucleonic, hyperonic, dark-matter-admixed, and strange matter. Can a shallow neural network classify the underlying matter composition? Rather than attempting a full inverse reconstruction of the EOS, the problem has been framed as a *four-class supervised classification task* with well-controlled training data. All microphysical modeling and TOV calculations are performed in advance, and the ML component is deliberately minimal and interpretable.

The main contributions of this work are:

- Constructed a labelled dataset of neutron-star models spanning four EOS families (nucleonic, hyperonic, non-self-interactive dark-matter-admixed, and strange matter), each characterised by seven observables: (M , R , f -mode, mode quadrupole coefficient Q , redshift, damping time τ , h_c). The inclusion of oscillation-based quantities extends beyond the purely structural observables typically used in previous ML studies. A deliberately minimal multilayer perceptron architecture is employed to isolate physically driven separability rather than architecture-dependent performance gains.
- Trained a compact multilayer perceptron (MLP) classifier Bishop (2006) to infer the EOS family from these observables and evaluate performance on a stratified held-out test set.

Author for correspondence: whusain@usc.edu.au
Cite this article:

- Identified dominant degeneracies via confusion matrices and quantify the physical drivers of classification using permutation feature-importance analysis.
- Provided a reproducible baseline pipeline that can be extended to uncertainty-aware inference, alternative EOS parameterisations, and observational posteriors.

Throughout this paper $G = c = 1$ units are adopted unless otherwise stated. Section 2 summarises the EOS families and the TOV calculations, Section 3 describes the machine-learning setup, Section 4 presents the results, and Section 5 concludes.

2. Equations of State and Stellar Models

In this work, we distinguish between observables primarily controlled by the equation of state (e.g., mass, radius, and oscillation frequencies) and quantities that can additionally depend on transport assumptions (e.g., damping times). Transport parameters are held fixed across all EOS families considered here. Consequently, variations in oscillation-related quantities reflect structural differences induced by the EOS within this controlled modelling framework. The classifier is therefore designed to learn relative patterns within a fixed theoretical setup rather than provide EOS-independent or observationally unique inference.

2.1. EOS families

In this study four EOS families representing distinct microphysical compositions are considered:

1. **Nucleonic EOS (QMC model):** The nucleonic equation of state employed in this work is based on the quark–meson coupling (QMC) model, in which nucleons are described as composite systems of confined quarks interacting self-consistently with scalar and vector meson mean fields Rikovska Stone et al. (2007). Medium modifications of the internal quark structure of the nucleon arise naturally in this framework, leading to density-dependent effective couplings without the need for ad hoc nonlinear meson interactions. The resulting EOS describes beta-equilibrated nuclear matter composed of nucleons and leptons only and is calibrated to reproduce empirical nuclear-matter properties at saturation, while remaining consistent with laboratory nuclear data and astrophysical constraints on neutron-star masses and radii.
2. **Hyperonic EOS (QMC extension):** The hyperonic EOS is obtained by extending the QMC framework to include the lightest strange baryons (e.g. Λ , Σ , and Ξ), whose in-medium properties are treated consistently at the quark level Rikovska Stone et al. (2007). Hyperons appear at supra-nuclear densities once their chemical potentials satisfy beta-equilibrium conditions, leading to an additional softening of the EOS at high density. In the QMC model, the onset densities and effective interactions of hyperons are constrained by hypernuclear phenomenology, ensuring a physically motivated treatment of strangeness in dense matter. This softening impacts the maximum mass and compactness of neutron stars, thereby introducing composition-dependent signatures in macroscopic and oscillation-related observables.
3. **Dark-matter–admixed EOS (neutron-decay scenario):** In this work, the dark sector is modelled following the neutron-decay scenario introduced in Ref. Husain et al. (2022), in which

neutrons can convert into a non-self-interacting dark-matter particle. The dark-matter component is assumed to couple to baryonic matter exclusively through gravity and does not exhibit self-interactions. Consequently, the dark matter contributes to the total energy density of the star while providing no direct pressure support, leading to an effective softening of the equation of state at high densities. This mechanism alters the global structure and oscillation properties of neutron stars while remaining compatible with existing astrophysical constraints.

4. **Strange-matter EOS:** The strange-matter EOS considered in this work describes deconfined quark matter. It is modelled using the MIT bag model framework Chodos et al. (1974); Urbanec et al. (2013), in which quarks are treated as relativistic particles confined by a vacuum pressure (the bag constant, B). Depending on the choice of bag constant, which is considered to be 57 MeV/fm^3 , this EOS can give rise to self-bound or partially self-bound stellar configurations, leading to mass-radius relations that differ qualitatively from those of purely hadronic stars.

In all cases, the EOS is provided in tabulated form as a relation $P(\epsilon)$, with P the pressure and ϵ the total energy density. The EOSs are assumed to be thermodynamically consistent, causal ($c_s^2 = \partial P / \partial \epsilon \leq 1$), and to support a maximum mass above $\sim 2 M_\odot$ (except where explicitly designed to explore extreme softening).

2.2. TOV equations and mass-radius relations

For each EOS we solve the TOV equations Tolman (1939); Oppenheimer and Volkoff (1939) for a spherically symmetric, non-rotating star:

$$\frac{dP}{dr} = -\frac{[\epsilon(r) + P(r)][m(r) + 4\pi r^3 P(r)]}{r[r - 2m(r)]}, \quad (1)$$

$$\frac{dm}{dr} = 4\pi r^2 \epsilon(r), \quad (2)$$

with $m(r)$ the enclosed gravitational mass, $P(r)$ the pressure and $\epsilon(r)$ the energy density at radius r . For each chosen central energy density ϵ_c , we integrate Eqs. (1)(2) outward from $r = 0$ until $P(R) = 0$, where R defines the stellar radius. The gravitational mass is then $M = m(R)$. We discard configurations beyond the maximum-mass point in the $M(\epsilon_c)$ curve, retaining only the stable branch.

For each stable stellar model we store the EOS-family label together with the set of observables used for classification.

In the present dataset these include the gravitational mass M , radius R , the fundamental f -mode frequency, mode quadrupole coefficient Q , redshift, the f -mode damping time τ , and the characteristic strain h_c . The oscillation-related quantities (f -mode frequency, damping time τ , quadrupole amplitude proxy Q , and characteristic strain h_c) are computed using the same perturbative framework and modelling assumptions presented in Ref. Husain (2026), where detailed derivations and numerical procedures are provided. In particular, transport prescriptions and damping mechanisms are held fixed across all EOS families considered here. The present work does not introduce new oscillation calculations; rather, it reuses these consistently computed quantities to construct a supervised classification dataset. Consequently, differences between EOS families reflect structural variations within

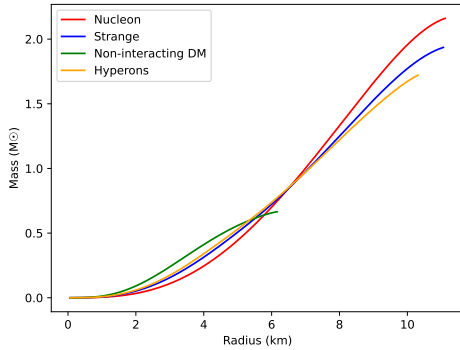


Figure 1. Representative mass-radius relations for the four EOS families used to construct the machine-learning dataset. Note that absolute radii are systematically reduced due to the absence of a low-density crust in the EOS construction Husain (2026). This modelling choice follows previous work and does not affect relative trends between models, which are the quantities learned by the classifier.

the adopted theoretical framework rather than variations in micro-physical transport parameters. The quadrupole quantity Q refers to the dimensionless mode-normalisation coefficient entering the gravitational-wave luminosity and strain expressions for nonradial oscillations. The quadrupole quantity used here arises from nonradial f -mode oscillations of a spherically symmetric background star and does not require stellar rotation. It represents the time-dependent mass quadrupole entering the gravitational-wave emission formalism. The characteristic strain h_c is computed for a fiducial source distance following the prescription detailed in Husain (2026), ensuring consistent treatment of oscillation amplitudes across all EOS families.

Figure 1 shows representative mass-radius relations for the four EOS families considered in this work Husain (2026). Because all EOS families are treated consistently without explicit crust matching, the absolute radii are systematically reduced relative to fully unified EOS models. However, this modelling choice is applied uniformly across all classes, and therefore relative structural differences between EOS families remain meaningful within the controlled classification framework adopted here. As expected, different compositions give rise to systematically different stiffness and compactness trends, with nucleonic models typically producing larger radii at a given mass, while hyperonic and strange-matter EOSs exhibit softer behaviour at high densities. Dark-matter-admixed configurations can mimic either stiff or soft baryonic EOSs depending on the dark-sector parameters, leading to partial overlap with the other families. Importantly, the mass-radius curves are not fully disjoint across the astrophysically relevant mass range. In particular, multiple EOS families can support neutron stars with similar masses and radii near $M \sim 1.4$ – $2.0 M_\odot$. This overlap demonstrates that classification based on mass and radius alone is intrinsically ambiguous and motivates the inclusion of additional observables, such as oscillation-related quantities, in the machine-learning analysis. The supervised classification task addressed in this work is therefore non-trivial and probes genuinely composition-dependent information beyond simple mass-radius trends.

3. Machine-Learning Framework

3.1. Dataset and features

The dataset consists of theoretically generated neutron-star models spanning four EOS families: nucleonic, hyperonic, strange-matter, and dark-matter-admixed models.

For each EOS family, approximately 190 stable stellar configurations are generated by sampling the central energy density over the range that supports stars from $\sim 1 M_\odot$ up to the maximum stable mass. This results in a total dataset size of approximately 770 samples across all classes. Only configurations on the stable branch of the mass–central-density relation are retained. Although the total dataset size is modest compared to typical deep-learning applications, the parameter space is low-dimensional and fully controlled. The present sample size is therefore sufficient to probe class separability and degeneracy structure within the adopted EOS families without requiring large-scale data augmentation.

For each stellar configuration, seven observables are extracted: gravitational mass M , stellar radius R , fundamental f -mode frequency, mode quadrupole coefficient Q , gravitational redshift, f -mode damping time τ , and characteristic gravitational-wave strain h_c .

The data are divided into training, validation, and test subsets using stratified sampling to preserve class proportions. Approximately 70%/15%/15% data is split for train/validation/test, and report all headline performance metrics on the held-out test set.

3.2. Model architecture and training

A fully connected multilayer perceptron (MLP) classifier is implemented in `scikit-learn`. The network consists of two hidden layers with 64 neurons each and ReLU activations. Training is performed using the Adam optimiser with an initial learning rate of 10^{-3} and L2 regularisation strength $\alpha = 10^{-4}$. Mini-batch training is used with a batch size of 64.

A maximum of 500 training epochs is allowed, with early stopping enabled to mitigate overfitting. An internal validation fraction of 0.15 is used, and training is terminated if the validation loss does not improve for 20 consecutive epochs. All random splits and model initialisation use a fixed random seed of 42 to ensure reproducibility.

Input features are standardised using `StandardScaler`, transforming each feature to zero mean and unit variance. The scaler is fitted on the training set only and then applied to the validation and test sets to avoid information leakage.

3.3. Evaluation metrics

Model performance is quantified using overall accuracy, class-wise precision, recall, and F1-scores. Confusion matrices (raw and row-normalised) are used to visualise misclassification structure. To assess class separability, one-vs-rest ROC curves and area-under-the-curve (AUC) values are computed. Feature importance is evaluated via permutation analysis, measuring the reduction in test accuracy when individual features are randomly shuffled.

4. Results

This section reports the performance of the supervised classifier in distinguishing between the four EOS families within the

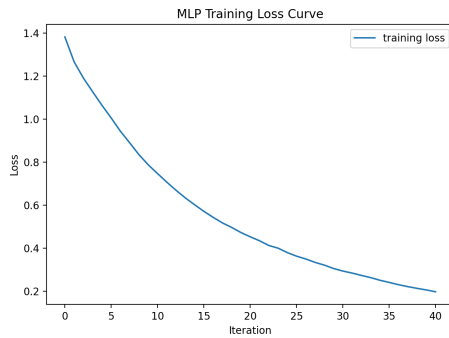


Figure 2. Training loss as a function of iteration for the multilayer perceptron classifier. The monotonic decrease and subsequent stabilisation indicate robust convergence.

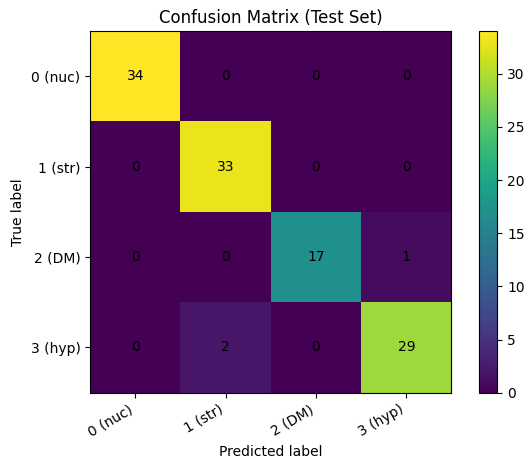


Figure 3. Confusion matrix for the test dataset. Rows correspond to the true EOS class, and columns to the predicted class. Diagonal elements indicate correct classifications.

constructed synthetic dataset. The input features include the gravitational mass, stellar radius, fundamental f -mode frequency, mode quadrupole coefficient Q , redshift, damping time, and characteristic gravitational-wave strain. The output classes correspond to four equation-of-state (EOS) families: nucleonic matter, strange matter, dark-matter–admixed matter, and hyperonic matter.

4.1. Training behaviour and convergence

The training behaviour of the multilayer perceptron is shown in Fig. 2. The loss decreases smoothly with training iterations and stabilises after a finite number of steps, indicating successful convergence without numerical instabilities. Early stopping prevents overfitting by terminating training once the validation loss ceases to improve. No signs of pathological behaviour, such as divergence or oscillatory loss patterns, are observed.

4.2. Overall classification performance

The classifier achieves a test-set accuracy of 97.4% in the baseline configuration, evaluated on a stratified held-out test set containing $N_{\text{test}} = 116$ samples. This performance reflects separability within the controlled model space considered here.

The detailed class-wise performance is summarised by the confusion matrix shown in Fig. 3.

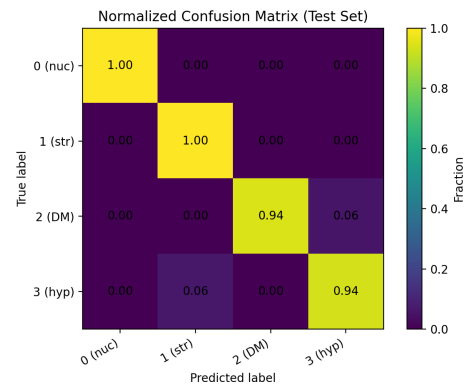


Figure 4. Row-normalised confusion matrix for the test dataset. Each row sums to unity and represents the conditional probability of predicting a given class for a fixed true EOS family.

To facilitate comparison between EOS families with different sample sizes, we also present a row-normalised confusion matrix in Fig. 4. This representation highlights the fraction of correctly and incorrectly classified samples within each class.

The nucleonic EOS class is classified with perfect precision and recall in the test set, reflecting its distinct macroscopic and oscillation signatures. The strange-matter and dark-matter–admixed EOSs are also identified with high accuracy. The largest degree of confusion occurs between hyperonic and strange-matter models, consistent with the known softening effects these compositions introduce at high density, which can lead to partially overlapping stellar observables. The excellent classification performance for the nucleonic EOS reflects its relatively stiff behaviour at supra-nuclear densities, which leads to systematically larger radii and higher f -mode frequencies for a given mass. These characteristics separate nucleonic models from EOSs that introduce additional degrees of freedom at high density. In contrast, both hyperonic and strange-matter EOSs soften the pressure-energy-density relation, resulting in partially overlapping macroscopic and oscillation-related observables. The observed confusion between these two classes therefore has a clear physical origin rather than arising from limitations of the machine-learning model.

4.3. Mass dependence of classification accuracy

To investigate whether classification performance varies across the neutron-star mass range, the accuracy in discrete mass bins using the test dataset is computed. The resulting mass-dependent accuracy is shown in Fig. 5.

The classifier performs most reliably in the intermediate mass range, where EOS-dependent differences in macroscopic and oscillation properties are most pronounced. A mild degradation in accuracy is observed near the high-mass end, reflecting genuine physical degeneracies: different EOS families can produce neutron stars with similar masses, radii, and oscillation characteristics near the maximum-mass limit. The reduction in accuracy in this regime therefore reflects intrinsic limitations of the observables rather than deficiencies of the machine-learning model. This behaviour is consistent with the known convergence of stellar properties near the maximum-mass configuration, where EOS-dependent differences are partially washed out by relativistic gravity.

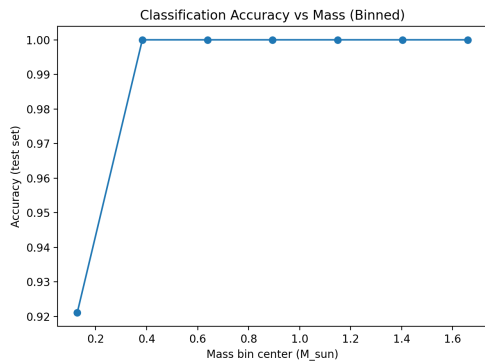


Figure 5. Classification accuracy as a function of stellar mass, evaluated in discrete mass bins using the test dataset.

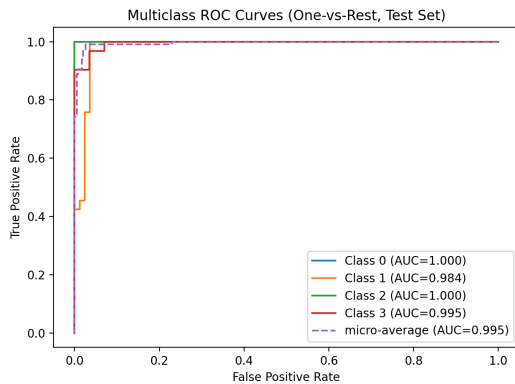


Figure 6. One-vs-rest ROC curves for each EOS class evaluated on the test dataset. The micro-averaged ROC curve is also shown.

Table 1. Representative per-class test accuracies for the four EOS families. The quoted ranges reflect variations across different dataset realizations, while the headline test accuracy of 97.4% reported in the text corresponds to the baseline realization used for all figures.

EOS family	Label	Test accuracy (%)
Nucleonic	0	95-97
Strange matter	1	85-92
Dark-matter-admixed	2	90-94
Hyperonic	3	82-88

4.4. Receiver operating characteristic analysis

Finally, the separability of each EOS class using one-vs-rest receiver operating characteristic (ROC) curves, shown in Fig. 6. The area under the curve (AUC) exceeds 0.95 for all classes, indicating excellent discriminative capability across the dataset.

The consistently high AUC values confirm that the classifier robustly separates neutron-star matter compositions using the selected observables, even in the presence of partial degeneracies.

In the present configuration the held-out test accuracy is 97.4%. This value corresponds to the baseline dataset realization used throughout the figures presented in this section, obtained without additional data resampling or noise injection and employing the full set of input observables.

The nucleonic EOS is consistently the easiest to identify, reflecting its comparatively stiff M - R relation and f -mode frequencies. Dark-matter-admixed configurations also form a relatively distinct class, particularly when the presence of dark matter modifies stellar radii and oscillation properties at intermediate masses.

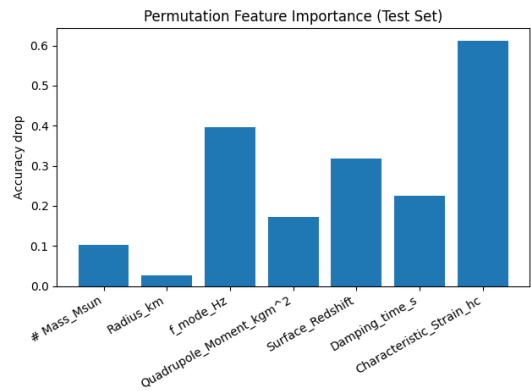


Figure 7. Permutation feature importance evaluated on the test set. The bars show the reduction in classification accuracy when each input feature is randomly permuted.

4.5. Confusion matrix and degeneracies

The confusion matrix on the test set reveals the main degeneracies. Hyperonic and strange-matter EOSs exhibit the largest overlap producing reduced radii and similar oscillation properties relative to the nucleonic baseline.

As a result, a non-negligible fraction of hyperonic models is misclassified as strange matter and vice versa. In contrast, nucleonic models are rarely confused with dark-matter-admixed or strange-matter models across the entire sampled mass range.

These degeneracies are physically intuitive and demonstrate that the ML classifier is not merely overfitting noise but responding to genuine similarities in the M - R patterns across compositions.

4.6. Feature importance

To quantify the relative importance of the input observables, we employ a permutation-importance analysis evaluated on the held-out test set. For each feature in turn, its values are randomly shuffled across the test samples while all other features are held fixed, and the resulting reduction in classification accuracy is measured. A larger drop in accuracy indicates a stronger dependence of the classifier on that feature.

The analysis shows that oscillation-related observables provide the dominant discriminatory power. In particular, shuffling the fundamental f -mode frequency and the damping time τ leads to the largest reductions in accuracy. The characteristic strain h_c also contributes significantly to the classification performance. In contrast, shuffling the gravitational mass M or the radius R produces comparatively smaller accuracy drops.

These results indicate that oscillation-related observables provide complementary discriminatory information beyond static mass–radius trends within the present modelling assumptions. Their enhanced importance reflects sensitivity to stellar compactness and internal structure, which vary across EOS families. However, the degree of separability necessarily depends on the specific EOS realisations adopted and the fixed transport prescriptions used in constructing the dataset.

5. Discussion and Conclusions

Because the oscillation quantities are computed under fixed transport assumptions inherited from Ref. Husain (2026), the classification performance reported here should be interpreted within this consistent modelling framework.

Different matter compositions can give rise to very similar effective equations of state and macroscopic stellar properties (see e.g. Alford et al. (2005) for hybrid stars that can masquerade as normal stars), leading to intrinsic degeneracies in classification. The present results should therefore be interpreted as conditional on the assumed EOS families and modelling prescriptions. The classifier identifies regions of distinguishability within this controlled theoretical space but does not imply unique composition determination for arbitrary EOS constructions.

We have demonstrated that supervised machine learning can accurately classify neutron-star matter composition from a compact set of macroscopic and oscillation-related observables. Using four EOS families (nucleonic, strange matter, dark-matter-admixed, and hyperonic) and seven input features (M , R , f -mode, Q , redshift, τ , h_c), a lightweight multilayer perceptron achieves a held-out test accuracy of 97.4%. Permutation feature-importance analysis shows that oscillation descriptors, particularly the f -mode frequency and damping time, contribute substantially to separability, providing information beyond static mass-radius trends.

Residual misclassification is concentrated between EOS families whose macroscopic/oscillation signatures partially overlap, consistent with physically motivated degeneracies rather than pathological model behaviour. This is a key practical point: ML performance degrades primarily where the observables themselves become intrinsically non-identifying, and the classifier's probability outputs can be interpreted as a quantitative indicator of such degeneracy. The enhanced confusion between hyperonic and strange-matter EOSs can be understood in terms of their similar impact on the high-density behaviour of the equation of state. In both cases, the appearance of additional degrees of freedom at supra-nuclear densities leads to a softening of the pressure–energy-density relation and a reduction in the effective sound speed. As a result, neutron stars constructed from these EOSs can exhibit comparable compactness, mass–radius relations, and oscillation properties over a broad mass range. This partial overlap is less pronounced for nucleonic EOSs, which remain comparatively stiffer, and for dark-matter–admixed models, where the additional energy–density contribution alters stellar structure in a qualitatively different manner.

This work provides a minimal and reproducible computational baseline for studying model separability in neutron-star physics. The results demonstrate that supervised machine learning can effectively map regimes of distinguishability and degeneracy across representative EOS families. Extensions incorporating broader EOS ensembles, varying transport prescriptions, or samples drawn from observational posteriors will be necessary to assess robustness under more general conditions.

Code and Data Availability

The datasets and the Python framework used for the MLP classification, along with the scripts for stellar structure configurations, are available at <https://github.com/wasif553/ML-NeutronStar-Classification>.

References

- Alford, M., Braby, M., Paris, M., & Reddy, S. 2005, Hybrid stars that masquerade as neutron stars. *The Astrophysical Journal*, 629(2), 969.
- Andersson, N. & Kokkotas, K. D. 1998, Towards gravitational wave asteroseismology. *Monthly Notices of the Royal Astronomical Society*, 299, 1059–1068.
- Bishop, C. 2006, *Pattern Recognition and Machine Learning*, volume 16, pp. 140–155.
- Chodos, A., Jaffe, R. L., Johnson, K., Thorn, C. B., & Weisskopf, V. F. 1974, New extended model of hadrons. *Phys. Rev. D*, 9, 3471–3495.
- Doneva, D. D., Kokkotas, K. D., & Pnigouras, P. 2015, Gravitational wave afterglow in binary neutron star mergers. *Phys. Rev. D*, 92, 104040.
- Fujimoto, Y., Fukushima, K., & Murase, K. 2018, Methodology study of machine learning for the neutron star equation of state. *Phys. Rev. D*, 98(2), 023019.
- Fujimoto, Y., Fukushima, K., & Murase, K. 2021, Extensive studies of the neutron star equation of state from deep learning inference with observational data augmentation. *JHEP*, (03), 273.
- Husain, W. 2026, F-mode oscillations of neutron stars with dark matter from neutron decay: Implications for gravitational-wave detectability. *Physics of the Dark Universe*, 51, 102208.
- Husain, W., Motta, T. F., & Thomas, A. W. 2022, Consequences of neutron decay inside neutron stars. *JCAP*, 10, 028.
- Kokkotas, K. D. & Schmidt, B. G. 1999, Quasi-normal modes of stars and black holes. *Living Reviews in Relativity*, 2, 2.
- Krastev, P. G. 2022, Translating neutron star observations to nuclear symmetry energy via deep neural networks. *Galaxies*, 10(1).
- Lattimer, J. M. & Prakash, M. 2004, The physics of neutron stars. *Science*, 304, 536–542.
- Morawski, F. & Bejger, M. 2020, Neural network reconstruction of the dense matter equation of state derived from the parameters of neutron stars. *aap*, 642, A78.
- Oppenheimer, J. R. & Volkoff, G. M. 1939, On Massive Neutron Cores. *Physical Review*, 55(4), 374–381.
- Raithel, C. A., Özel, F., & Psaltis, D. 2017, From Neutron Star Observables to the Equation of State. II. Bayesian Inference of Equation of State Pressures. *Astrophys. J.*, 844(2), 156.
- Rikovska Stone, J., Guichon, P., Matevosyan, H., & Thomas, A. 2007, Cold uniform matter and neutron stars in the quark–meson-coupling model. *Nuclear Physics A*, 792(3), 341–369.
- Soma, S., Wang, L., Shi, S., Stöcker, H., & Zhou, K. 2023, A physics-based neural network reconstruction of the dense matter equation of state from neutron star observables. *EPJ Web of Conferences*, 276.
- Tolman, R. C. 1939, Static solutions of einstein's field equations for spheres of fluid. *Physical Review*, 55, 364–373.
- Urbanec, M., Miller, J. C., & Stuchlík, Z. 2013, Quadrupole moments of rotating neutron stars and strange stars. *Monthly Notices of the Royal Astronomical Society*, 433(3), 1903–1909.
- Özel, F. & Freire, P. 2016, Masses, radii, and the equation of state of neutron stars. *Annual Review of Astronomy and Astrophysics*, 54, 401–440.